Available online at www.sciencedirect.com
ScienceDirect
Deep-Sea Research II 55 (2008) 901–912
DEEP-SEA RESEARCH PART II
www.elsevier.com/locate/dsr2

Modelling the effect of iron fertilization on dimethylsulphide emissions in the Southern Ocean

Laurent Bopp[a,*], Olivier Aumont[b], Sauveur Belviso[a], Stéphane Blain[c]

[a]IPSL/Laboratoire des Sciences du Climat et de l'Environnement, CEA/CNRS/UVSQ, CEN de Saclay, Bât 701 l'Orme des Merisiers, 91191 Gif-sur-Yvette, France
[b]IPSL/Laboratoire d'Océanographie: Expérimentation et Approche Numérique, CNRS/UPMC/IRD, Centre IRD de Bretagne, BP 70, 29280 Plouzané, France
[c]Aix-Marseille Université; CNRS; LOB-UMR 6535, Laboratoire d'Océanographie et de Biogéochimie, OSU/Centre d'Océanologie de Marseille, France

Accepted 11 December 2007
Available online 7 April 2008

Abstract

In this study, we use a 3D ocean biogeochemical model to explore the relationship between iron fertilization and dimethylsulphide (DMS) production in the Southern Ocean. The model is able to reproduce the observed decoupling between high productivity and DMS-rich waters because the main processes (variable sulphur-to-carbon ratio in phytoplankton, variable transfer efficiency from DMS precursor to DMS, and variable bacterial DMS-consumption rate) are taken into account. Moreover, the model predicts that a 20-yr iron fertilization of the entire Southern Ocean would actually reduce the emissions of DMS to the atmosphere.

Keywords: Dimethylsulphide; DMS; DMSP; Iron; Southern Ocean; Modelling

1. Introduction

Dimethylsulphide (DMS) is produced by the degradation of dimethylsulphoniopropionate (DMSP), which is released by marine phytoplankton, and can exchange with the atmosphere. It has been proposed that marine emissions of DMS from the Southern Ocean are sensitive to climatic change and that the radiative budget of the Earth will be sensitive to such changes (Charlson et al., 1987; Legrand et al., 1998; Bopp et al., 2004; Larsen, 2005; Gunson et al., 2006). It is therefore crucial to understand the biogeochemistry of DMS in the Southern Ocean and the impact of changes in environmental factors. All field experiments have demonstrated the pivotal role of iron in controlling both biological productivity and nutrient utilization in the Southern Ocean (de Baar et al., 2005 and references therein). Additionally, dissolved iron (dFe) enrichments have always led to a marked increase in DMS concentrations (Turner et al., 2004; Wingenter et al., 2004; Liss et al., 2005). Although it is clear that the addition of dFe stimulates short-term DMS production, such experiments have been carried out for at most several weeks. Therefore it is unknown if DMS production would continue to be stimulated over longer time scales.

In a recent paper reporting on the subarctic Pacific SERIES experiment, Levasseur et al. (2006) confirmed the rapid increase in DMS concentrations following dFe enrichment. However, a unique and significant decrease in DMS concentrations was measured inside the dFe patch a few days after the initial dFe addition and associated DMS increase (Levasseur et al., 2006). Utilizing an inverse modelling approach, Le Clainche et al. (2006) were able to reconstruct the net DMS production during SERIES. After the initial increase in nanophytoplankton abundance and DMSP, iron enrichment reduced the DMS production efficiency of the microbial system, leading to net DMS consumption during the diatom bloom (Le Clainche et al., 2006) and to a decoupling between iron enrichment and DMS concentrations. Therefore it is possible that the addition of dFe to HNLC waters may not always lead to enhanced DMS production that could mitigate climate warming.

*Corresponding author.
E-mail address: Laurent.Bopp@lsce.ipsl.fr (L. Bopp).

0967-0645/$ - see front matter © 2008 Elsevier Ltd. All rights reserved.
doi:10.1016/j.dsr2.2007.12.002

A similar decoupling between productivity and DMS concentrations has been observed by Belviso et al. (2008) in the Indian sector of the Southern Ocean. The authors show that the sustained enrichment of iron over the Kerguelen Plateau does not translate into an increase in DMS concentrations. Three mechanisms were invoked to explain this result: (1) the small eukaryotes, which are the main producers of particulate DMSP (pDMSP), are not favoured by the continuous supply of dFe in surface waters, (2) the transfer efficiency of DMSP to DMS would be lower and the DMS removal higher on than off the plateau, probably due to the higher levels of bacterial production measured on the plateau, and (3) the supply of deep waters rich in nitrates and chromophoric dissolved organic matter (DOM) associated with iron increase the photodegradation rates of DMS.

To provide further insight into the impact of iron fertilization on DMS emissions, we use the biogeochemical model Pelagic Interactions Scheme for Carbon and Ecosystem Studies (PISCES; Aumont and Bopp, 2006). PISCES is a 3D biogeochemical model that explicitly represents the oceanic iron and sulphur cycles. In contrast to the modelling study of Le Clainche et al. (2006), our goal here is not to develop an integrated dynamical budget of DMS on the Kerguelen Plateau. Instead, we explore the links between iron fertilization and DMS production on a larger scale (both in time and space). To this end, we use PISCES to examine (1) the climatological distribution of DMS in the Southern Ocean, (2) the response of DMS to patchy iron-fertilization experiments, and finally (3) the response of DMS to a 20-yr-long iron addition in HNLC waters of the Southern Ocean.

2. Methods

2.1. Description of the DMS model

PISCES is a 3D biogeochemical model that simulates marine biological productivity and describes the biogeochemical cycles of carbon and of the main nutrients (P, N, Si, Fe), as well as two phytoplankton and two zooplankton functional groups. PISCES was designed to be used over a wide range of spatial and temporal scales (see Bopp et al., 2003, 2005; Gorgues et al., 2005; Aumont and Bopp, 2006). A complete description of PISCES can be found in Aumont and Bopp (2006) and a release of the model is available to the community (www.lodyc.jussieu.fr/NEMO). For the purpose of this study, a prognostic module computing DMS seawater concentrations and DMS air–sea fluxes was imbedded within PISCES. Here, we only describe the equations and parameters used in this module. The set of parameters used for the sulphur cycling are summed up in Table 1.

The DMS cycle module explicitly simulates the two compounds pDMSP and DMS according to the following equations:

$$\mathrm{pDMSP} = \sum_i \left(\frac{S}{C}\right)^i C_i, \tag{1}$$

$$\frac{\partial\,\mathrm{DMS}}{\partial t} = \sum_i [G_i + E_i + M_i]\left(\frac{S}{C}\right)^i Y_\mathrm{S} - \lambda^*_\mathrm{DMS}\,\mathrm{DMS} - \lambda^\mathrm{PAR}_\mathrm{DMS}\,\mathrm{PAR}\,\mathrm{DMS} - k_\mathrm{g}\,\mathrm{DMS}, \tag{2}$$

where the subscript i represents the two phytoplankton groups in PISCES, diatoms and nanophytoplankton. The different terms of these two equations are described below.

In Eq. (1), pDMSP is computed from the carbon biomass of the two groups (diatoms and nanophytoplankton) via group-specific sulphur (DMSP)-to-carbon (S/C) ratios (Steffels et al., 2007). Recent studies have highlighted large variability in S/C ratio within a specific phytoplankton group as a function of environmental factors (Sunda et al., 2002; Bucciarelli and Sunda, 2003). Bucciarelli et al. (2007) have shown for *Emiliana huxleyi* that the ratios of intracellular DMSP to other biomass parameters (C, N, and Chla) decreased during the day and increased at night.

Table 1
Model coefficients related to the DMS cycle with their standard values in PISCES and references

Parameter	Unit	Value	Description	Reference
a	d^{-1}	0.66	Growth rate at 0 °C for nanophyto., diatoms, and bacteria	Aumont and Bopp (2006)
b	–	1.066	Temperature sensitivity of growth	Aumont and Bopp (2006)
K_{PO_4}	μM P	0.0008/0.004/0.0008	PO_4 half-saturation constants: nano/diatoms/bacteria	Aumont and Bopp (2006)
K_{NH_4}	μM N	0.013/0.065/0.013	NH_4 half-saturation constants: nano/diatoms/bacteria	Aumont and Bopp (2006)
K_{NO_3}	μM N	0.26/1.3	NO_3 half-saturation constants: nano/diatoms	Aumont and Bopp (2006)
K_Si	μM Si	2	Si half-saturation constant for diatoms	Aumont and Bopp (2006)
K_Fe	nM Fe	0.02/0.1/0.02	Minimum Fe half-saturation constant for: nano/diatoms/bacteria	Aumont and Bopp (2006)
$(S/C)^\mathrm{D}$	mol S (mol C)$^{-1}$	0.0018	S-to-C ratio of diatoms	Steffels et al. (2007)
$(S/C)^\mathrm{P}_\mathrm{min}$	mol S (mol C)$^{-1}$	0.015	Minimum S-to-C ratio of nano	Steffels et al. (2007)
$(S/C)^\mathrm{P}_\mathrm{var}$	mol S (mol C)$^{-1}$	0.015	S-to-C ratio coefficient of nano	Sunda et al. (2002)
$Y_\mathrm{S\,min}$	–	0.2	Minimum dDMSP-to-DMS yield	Vezina (2004)
$Y_\mathrm{S\,var}$	–	0.4	dDMSP-to-DMS yield coefficient	Kiene et al. (2000)
$\lambda^\mathrm{B}_\mathrm{DMS}$	d^{-1}	0.2	DMS loss rate by bacterial activity	Kieber et al. (1996)
K_DMS	nM S	1.5	Half-saturation constant of DMS loss to bacterial consumption	This study
$\lambda^\mathrm{PAR}_\mathrm{DMS}$	d^{-1} (W m^{-2})$^{-1}$	0.05	Photochemical loss rate	Vezina (2004)

Due to the low diatom S/C ratio used here, our model was insensitive to variability in this parameter for the diatom group (data not shown). Therefore, diatom S/C ratio is fixed. For nanophytoplankton, we employ a variable S/C ratio that increases in response to stress from low nutrient concentrations and high UV radiation (Sunda et al., 2002):

$$L_{UV} = \frac{1}{1 + \max(0., \mathrm{PAR} - 30.)}, \quad (3)$$

$$L^{P}_{lim} = \min(L^{P}_{PO_4}, L^{P}_{NO_3}, L^{P}_{NH_4}, L^{P}_{Fe}), \quad (4)$$

where $L^{P}_{x} = [x]/(K_x + [x])$,

$$\left(\frac{S}{C}\right)^{P} = \left(\frac{S}{C}\right)^{P}_{min} + \left(\frac{S}{C}\right)^{P}_{var} (1 - \min(L^{P}_{lim}, L_{UV})). \quad (5)$$

As the UV radiation level is not explicitly computed in PISCES, we assume that high PAR is associated with high UV levels in order to compute the L_{UV} term in Eq. (3). In Eq. (4), L^{P}_{lim} denotes the limitation of nanophytoplankton growth by nutrients (dFe, NO_3^-, NH_4^+ and PO_4^{3-}). In Eq. (5), $(S/C)_{min}$ and $(S/C)_{var}$ are two parameters representing the minimum and the variable part of the S/C ratio for nanophytoplankton, so that S/C can vary between 0.015 and 0.030. Furthermore, the S/C ratio in phytoplankton is assumed to adapt instantaneously to the local conditions. Accordingly, pDMSP can be directly diagnosed from the phytoplankton biomass (C_i) as there is no decoupling between the carbon and the sulphur contents of the phytoplankton cells.

In Eq. (2), pDMSP is released to the water column as dissolved DMSP (dDMSP) via three different processes: grazing by zooplankton (G_i), exudation by phytoplankton (E_i), and phytoplankton cell lysis (M_i). These terms are modelled as per Lefèvre et al. (2002): in short, all pDMSP grazed by zooplankton is released to seawater, the exudation of dDMSP is similar to that of DOM, and the cell lysis is computed from phytoplankton mortality.

Once released into water, we assume that bacterial activity instantaneously transforms dDMSP into DMS. Consequentially, dDMSP is not explicitly modelled in PISCES. The dDMSP-to-DMS yield (percentage of cleavage) has been shown to vary both spatially and temporally by between 0% and 100% (Simó and Pedros-Alio, 1999). Vezina (2004) has reported values of dDMSP-to-DMS yield (18–68%) that have been used among published DMS ecosystem models. In addition, Kiene et al. (2000) have shown that the dDMSP-to-DMS yield increases with bacterial nutrient stress. To estimate the dDMSP-to-DMS yield Y_S, we have adopted the following empirical parameterization:

$$L^{B}_{lim} = \min(L^{B}_{PO_4}, L^{B}_{NO_3} L^{B}_{NH_4}, L^{B}_{Fe}), \quad (6)$$

where $L^{B}_{x} = [x]/(K_x + [x])$,

$$Y_S = Y_{S\,min}\, Y_{S\,var}(1 - \min(L^{B}_{lim})). \quad (7)$$

In this set of Eqs. (6) and (7) L^{B}_{lim} is the bacterial nutrient stress factor, Y_S the dDMSP-to-DMS yield, and $Y_{S\,min}$ and $Y_{S\,var}$ are the minimum and the variable part of the yield, respectively. In short, the modelled dDMSP-to-DMS yield increases from 20% to 60% as a function of the bacterial nutrient stress as per Kiene et al. (2000).

In seawater, DMS is lost due to bacterial (λ^{*}_{DMS} DMS) and photochemical (λ^{PAR}_{DMS} PAR DMS) processes and ventilation to the atmosphere (k_g DMS). The bacterial consumption of DMS is parameterized as a function of the bacterial biomass (B) and activity ($L^{B}_{lim} b^{T}$):

$$\lambda^{*}_{DMS} = \lambda^{B}_{DMS} L^{B}_{lim} b^{T} B \frac{\mathrm{DMS}}{K_{DMS} + \mathrm{DMS}}. \quad (8)$$

This parameterization (Eq. (8)) is similar to the formulation adopted in PISCES to compute the remineralization rate of DOM (see Eq. (21) in Aumont and Bopp, 2006). The rate constant λ^{B}_{DMS} for bacterial consumption of DMS is set to $0.2\,d^{-1}$, which is in the low end of the range estimated by Kieber et al. (1996) for the equatorial Pacific ($0.2–0.6\,d^{-1}$).

The temperature dependence, b^{T}, is based on the power law of Eppley (1972) for phytoplankton. PISCES does not explicitly model bacterial biomass; it is estimated as a linear combination of the zooplankton biomass terms ($B = 0.7(Z + 2M)\min(1{,}120./z)$) where Z and M are the micro- and meso-zooplankton concentrations, respectively, and z is the depth. This relationship has been constructed from a version of PISCES that includes an explicit description of the bacterial biomass (see Aumont and Bopp, 2006). K_{DMS} has been adjusted from several sensitivity experiments (not shown) and is set to 1.5 nM.

The photochemical loss rate is a linear function of PAR. For the rate constant of photo-oxidation, λ^{PAR}_{DMS}, we use $0.05\,d^{-1}(W\,m^{-2})^{-1}$, similar to the value of $0.07\,d^{-1}(W\,m^{-2})^{-1}$ used by Lefèvre et al. (2002) and in the range of the values used in published ecosystem models (Vezina, 2004).

For ventilation to the atmosphere, the gas exchange coefficient, k_g, is computed using the relationship as per Wanninkhof (1992) and the Schmidt number for DMS calculated following the formula given by Saltzman et al. (1993).

2.2. Experimental design

We coupled our DMS model to the dynamical ocean model ORCA2-LIM, which is based on both the ORCA2 global configuration of OPA version 8.2 (Madec et al., 1998) and the dynamic–thermodynamic sea-ice model developed at Louvain-La Neuve (Fichefet and Morales Maqueda, 1997). The ocean model has a mean horizontal resolution of 2° by $2° \cos\phi$ (where ϕ is the latitude) with a meridional resolution that is enhanced to 0.5° at the equator. The model has 30 vertical levels (increasing from 10 m at the surface to 500 m at depth); 12 levels are located in the top 125 m.

In this study, we have used the same forcing fields as those of Aumont and Bopp (2006), as well as the same experimental design. We performed a climatological

simulation run to quasi-equilibrium (~3000 yr), patchy iron-fertilization experiments and a 20-yr long-term iron-fertilization performed in the Southern Ocean. For the patchy iron-fertilization experiments, the fertilizing sites are south of 40°S and iron was added to one grid cell every 10° in longitude and 5° in latitude. At each site, the dFe concentration was set to 2 nM throughout the whole mixed layer and maintained at that value for the rest of the simulation for a total duration of 45 d. Finally, large-scale and long-term iron fertilization was performed. In this experiment, dFe was set to 2 nM in the mixed layer south of 40°S and maintained to that value for 20 yr (starting in 2000). To perform iron-fertilization experiments (both small and large scale), we set the dFe concentration to 2 nM, close to the maximum concentrations reached in the fertilized patch during SOIREE (2–4 nM; Boyd et al., 2000). This concentration also alleviates iron limitation for both phytoplankton groups in the PISCES model.

3. Results and discussion

3.1. Climatological simulation

The objective of this section is not to present an exhaustive evaluation of the model results as many fields are evaluated elsewhere (Aumont and Bopp, 2006). We briefly compare the mean distribution of DMS concentrations in surface waters to previously published estimates based on observations and/or models. We then focus on the similarities between our model results and the findings of Belviso et al. (2008) on the relationship between dFe and DMS concentrations in the Southern Ocean.

A variety of different approaches have been utilized to examine oceanic DMS cycling on the global scale. Since the pioneering work of Erickson et al. (1990), a series of DMS monthly climatologies was proposed (Kettle et al., 1999; Kettle and Andreae, 2000; Anderson et al., 2001; Aumont et al., 2002; Simó and Dachs, 2002; Chu et al., 2003; Belviso et al., 2004). The Kettle et al. (1999) and Kettle and Andreae (2000) syntheses rely on the assemblage of a database of DMS measurements. In addition, Anderson et al. (2001) generated monthly global DMS fields using a relationship equating DMS to the product of chlorophyll, light, and nutrient terms. A similar approach was undertaken by Simó and Dachs (2002), where a double-equation algorithm with chlorophyll and mixed-layer depth was found to explain a large fraction of the variance for surface concentration. Aumont et al. (2002) and Belviso et al. (2004) made use of non-linear parameterizations to relate DMS concentration to chlorophyll and to an index of the community structure of marine phytoplankton representing the proportion of micro-phytoplankton within the whole phytoplankton community. Finally, Chu et al. (2003) used a reduced formulation of the production and removal processes of DMS, which was implemented into a high resolution ocean circulation model, to produce the first mechanistic global model of DMS. In that sense, the approach we present here is close to the one followed by Chu et al. (2003). These different monthly climatologies have been extensively compared by Belviso et al. (2004) and more recently by Bell et al. (2006).

The simulated DMS concentrations modelled for a climatological year compare reasonably well with all other estimates at the global scale (not shown). Low DMS concentrations are predicted in the subtropical gyres and higher concentrations are predicted in the equatorial pacific and at mid-to-high latitudes. In the Southern Ocean, large differences are found between the different approaches (Fig. 1). Our model predicts high concentrations (up to 5 nM) in the subtropical/subantarctic convergence, similar to those of Chu et al. (2003), Aumont et al. (2002) and Simó and Dachs (2002). Although this pattern does not appear in the Kettle and Andreae (2000) database, maximum DMS concentrations between 7 and 35 nM have been measured in the convergence zone of the Atlantic (Belviso et al., 2000) and Indian (Sciare et al., 2000) oceans. On the other hand, DMS concentrations are underestimated along the Antarctic coasts (as in all other climatologies except Kettle and Andreae, 2000) where PISCES does not explicitly resolve the strong blooms of *Phaeocystis*, a phytoplankton species that contributes heavily to local DMS production. To study seasonal variability, we also compared the annual cycle of zonal mean surface concentrations using latitude–time (Hövmöller) plots (Fig. 1). In agreement with almost all climatologies, our model predicts a strong seasonal cycle south of 60°S and a very weak seasonal cycle north of 60°S.

To quantitatively estimate how the DMS climatology produced here compares to previously published estimates and to the typical reference (Kettle and Andreae, 2000), we used the diagram of Taylor (2001) that compares frequently used statistics: the standard deviation, the correlation coefficient r, and the pattern root mean square (RMS) error (Fig. 2). We show those statistics for both the global ocean (black dots in Fig. 2) and the 30–90°S domain (white dots in Fig. 2). As shown by Belviso et al. (2004), there is a low correlation for the global space–time variation of surface DMS concentrations (r is always lower than 0.3) between the Kettle and Andreae (2000) data-based climatology and the five other climatologies discussed here (including our new estimate for which r is 0.18). For most of those climatologies, the standard deviation is substantially lesser than the standard deviation found in Kettle and Andreae (2000). When computed over 30–90°S, the correlation r between our estimate and the Kettle and Andreae (2000) database increases from 0.18 to 0.33 (Fig. 2), which is higher than for the four other climatologies (r between 0.12 and 0.27). But when computed over 30–90°S, the standard deviation is lower than that at the global scale (only 0.2 of the standard deviation found in Kettle and Andreae, 2000). This low normalized standard deviation is nevertheless a common feature of the other four climatologies and may be explained by the sharp contrasts both in time and space

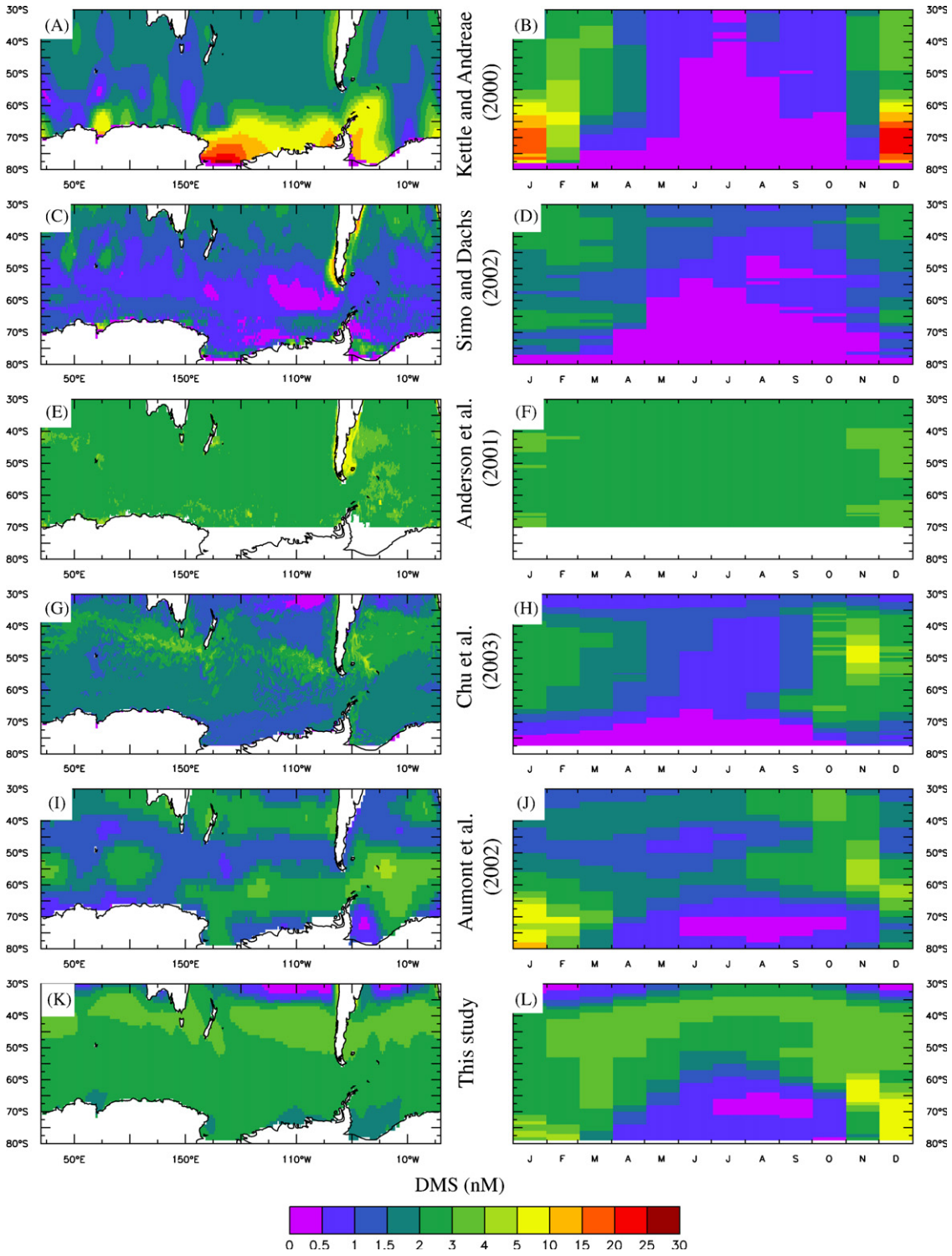

Fig. 1. DMS surface concentrations in nmol L^{-1}, annual mean (left), and zonal mean of the seasonal cycle (right). Panels (K) and (L) display our model results. Other panels show DMS surface distributions obtained either from a global dataset (panels A and B: Kettle and Andreae, 2000) or from various previously proposed parameterizations: (C) and (D) Simó and Dachs (2002), (E) and (F) Anderson et al. (2001), (G) and (H) Chu et al. (2003), (I) and (J) Aumont et al. (2002).

that are found in Kettle and Andreae (2000) for the Southern Ocean (Fig. 1).

In order to compare this climatological simulation to the results of Belviso et al. (2008), we have examined the relationship between high- or low-productivity waters and DMS-rich or -poor waters in the Southern Ocean. The results from our simulation show a decoupling between elevated productivity and DMS-rich waters in February (Fig. 3) and support the findings from Belviso et al. (2008). As measured during KEOPS (Fig. 3), low levels of pDMSP

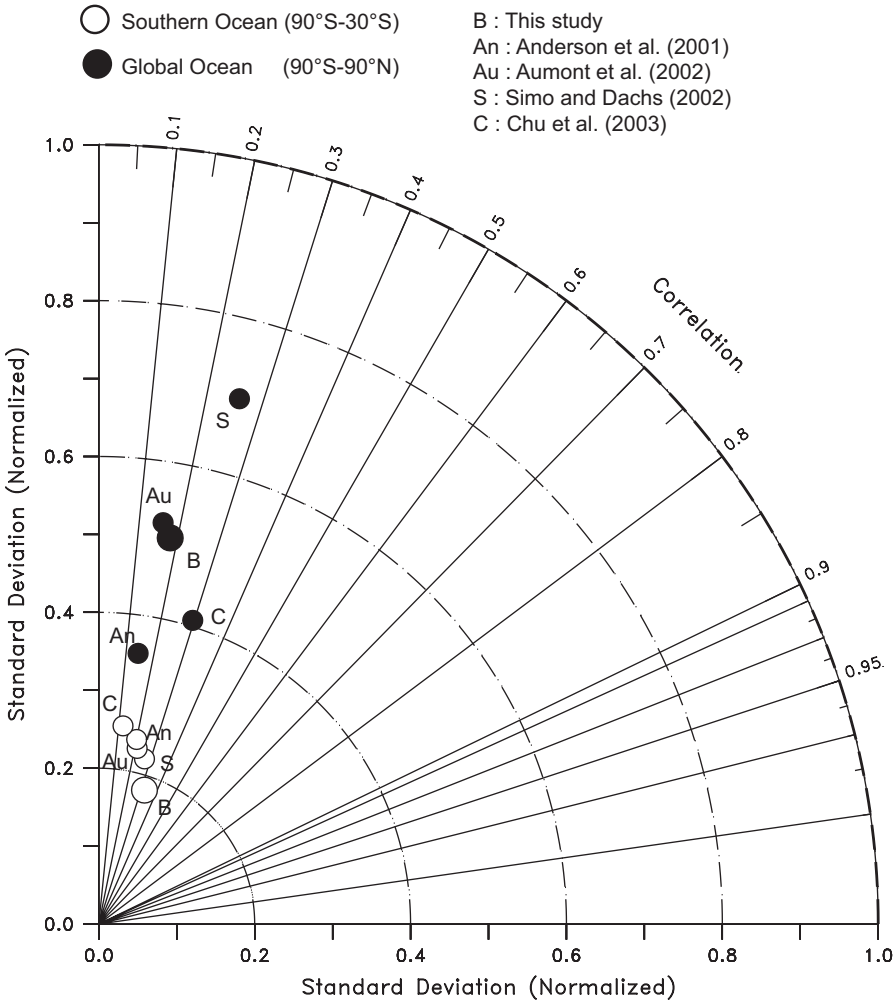

Fig. 2. Pattern statistics describing the total space–time variations in DMS concentrations as obtained from five gridded climatologies compared to Kettle and Andreae (2000). In this polar plot (Taylor, 2001), the radius corresponding to each label gives the normalized standard deviation, i.e. the ratio between the standard deviations of a given climatology and the reference climatology (Kettle and Andreae, 2000). The angular coordinate indicates the correlation coefficient r between a given climatology and the reference. The distance from the reference point to any label is the central root mean square (RMS) error.

and DMS (Figs. 3(C) and (D)) are simulated for both low (surface Chl $a < 0.2\,\mathrm{mg\,m^{-3}}$) and high (surface Chl $a > 1\,\mathrm{mg\,m^{-3}}$ with high diatom abundance, $>70\%$) productivity waters. In PISCES, this decoupling (high productivity and low DMS) is due to the low S/C cell quotas resulting from diatom dominance of the phytoplankton community, to the low transfer efficiency of dDMSP to DMS, and to the high rates of DMS removal by bacteria. These three processes act in concert to prevent accumulation of DMSP and DMS in surface waters when diatoms are abundant.

The two biogeochemical scenarios described above (i.e. either HNLC conditions or high phytoplankton biomass largely dominated by diatoms) both exhibit modest pDMSP and DMS concentrations. Although these scenarios are largely prevalent spatially and temporally in the Southern Ocean, high levels of pDMSP and DMS can be predicted by PISCES in the Southern Ocean. At the beginning of the growing season, the mixed-layer shoals and a bloom of both diatoms and nanophytoplankton ensues. The high S/C cell quota of the nanophytoplankton results in a significant buildup in pDMSP and DMS (up to 70 nM for pDMSP and up to 7 nM for DMS, Fig. 3, month of November). Intense microzooplankton grazing and exhaustion of iron quickly result in the collapse of the initial nanophytoplankton bloom and the system returns to one of the two stable conditions (low productivity and low DMS, high productivity and low DMS). To some extent, this early-bloom situation can be thought of as similar to the initial DMS buildup seen in artificial iron-fertilization experiments (Fig. 3, SOIREE).

3.2. Patchy iron fertilization in the Southern Ocean

PISCES also produces high DMS concentrations in the HNLC Southern Ocean during local patchy iron-fertilization experiments. The model behaviour is illustrated in Fig. 4 for sites similar in their physical conditions to those of the SOIREE experiment (Boyd et al., 2000). The chlorophyll, ecosystem structure and pCO_2 responses

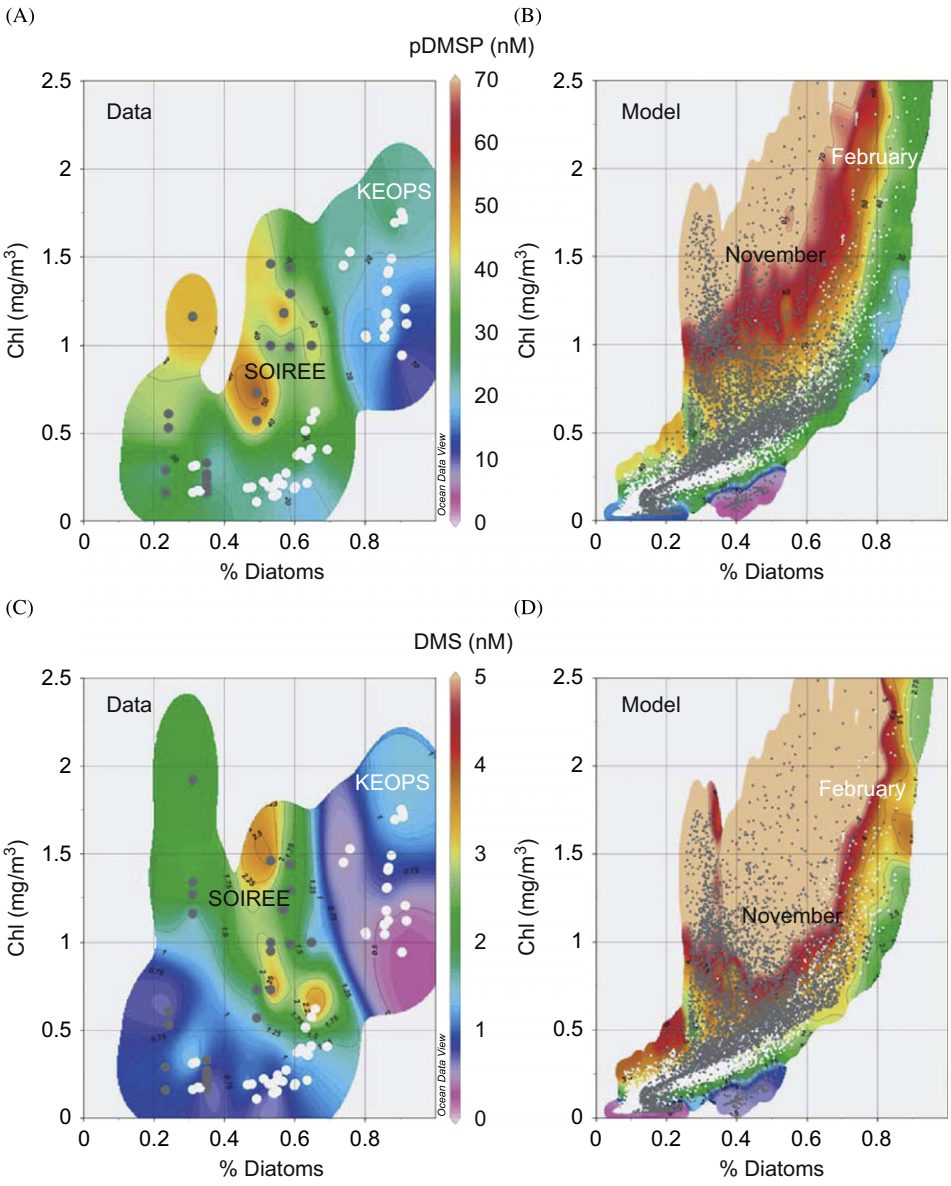

Fig. 3. Observed and simulated distributions of pDMSP and DMS concentrations. pDMSP (upper panels) and DMS (lower panels) concentrations in surface waters plotted against corresponding concentrations of Chl *a* and the relative contribution of diatoms to the phytoplankton pool. Left panels are constructed from observations of both the KEOPS (white dots) and SOIREE (grey dots) experiments. Right panels are constructed from modelled monthly means of surface concentrations for the months of February (white dots) and November (black dots) and for all the 30–90°S domain. The coloured contour plots are created by the same way for both the observations and the model: DMS and DMSP values are placed into bins given by the diatom abundance and chlorophyll concentrations and then averaged and interpolated.

were discussed in detail in Aumont and Bopp (2006). In brief, a strong and rapid increase in chlorophyll is simulated after fertilization that is similar in magnitude to the observations. In both PISCES and the observations, the maximum phytoplankton biomass is reached after ~20 d. Most of the increase in biomass is due to diatoms, which comprise more than 60% of the total phytoplankton biomass (Aumont and Bopp, 2006), in good agreement with the measurements (Gall et al., 2001). Due to the phytoplankton bloom, surface pCO_2 decreases significantly at all selected fertilization sites, in good agreement with observations (Bakker et al., 2001).

A large and rapid increase in pDMSP is simulated after fertilization, reaching a maximum of up to +20 nM after 4–5 d. This is then followed by a rapid decline over the subsequent 10 d. This behaviour is similar to that observed during SOIREE (Turner et al., 2004) although the model seems to slightly underestimate the peak in pDMSP (+30 nM in the observations vs. 0 to +20 nM in the model results). This underestimation is explained by the fact that the model overestimates the contribution of diatoms (low DMSP producers) in the biomass buildup that follows Fe fertilization. The up-to-3 nM increase in DMS simulated in PISCES is also followed by a rapid

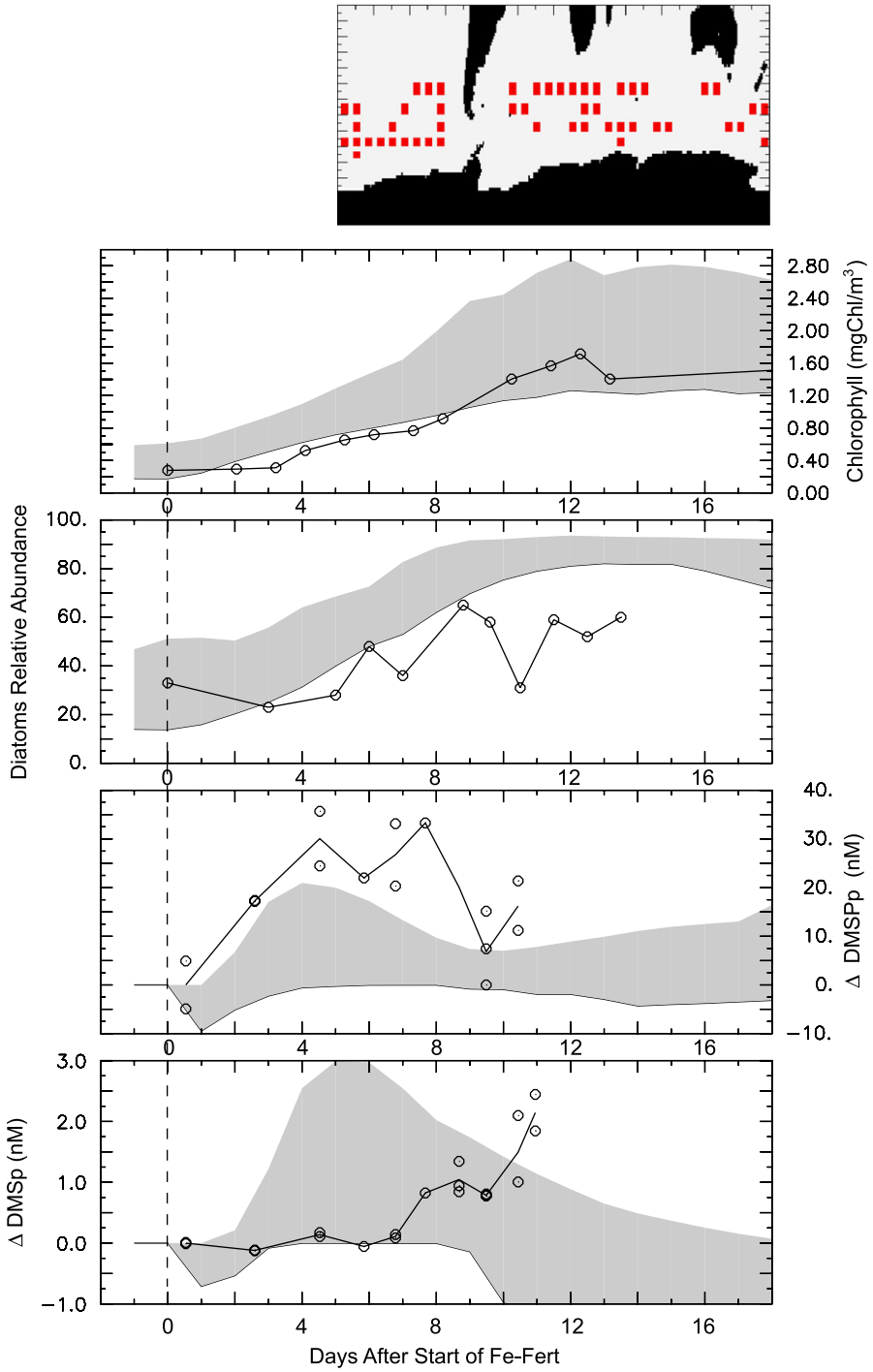

Fig. 4. Evolution of some biogeochemical signals (mean chlorophyll, diatoms contribution, surface pDMSP, and surface DMS) at SOIREE. The dots on all panels denote the observations. The grey shaded area indicates the range in the model responses: all the injection sites in the model that have similar mixed-layer depth (45–85 m) and SST (0–4 °C) to the SOIREE site (65 m and 2 °C, respectively) have been selected. Their locations are shown on the upper map. Iron has been added in the model at the same month as in the data (February). Both the model output and the observations are displayed so that the first iron infusion occurs on day 0. Chlorophyll (A) is expressed as mean mixed-layer concentrations. Diatom contribution (B) is shown as a percentage of the total Chl *a*. Differences in pDMSP (C) and DMS (D) are defined for the model and the observations as the differences between the fertilization experiment and a control experiment, and between in- and out-patch measurements, respectively. We have chosen to show differences for pDMSP and DMS concentrations because DMS and pDMSP concentrations in the model exhibit very different values at the start of the fertilization experiment.

decline to concentrations lower than in surrounding waters. This initial increase in DMS is comparable to that observed during SOIREE (Turner et al., 1999) for its amplitude, but the peak in DMS concentrations is 4–5 d earlier than observed (Fig. 4). The subsequent decline that is predicted by PISCES cannot really be compared to the SOIREE data as DMS measurements were only conducted for less than 10 d.

In PISCES, the initial iron addition triggers a bloom of both diatoms and nanophytoplankton and the high nanophytoplankton S/C cell quota results in a significant buildup in pDMSP and DMS. Then, microzooplankton grazing or nutrient exhaustion result in the collapse of this initial nanophytoplankton bloom and the rapid decline in DMSP and DMS concentrations. Iron enrichment also reduces the DMS production efficiency of the microbial system (up to −15%) and increases the bacterial consumption of DMS (up to +250%) as a result of relief of nutrient limitation of bacterial activity (via the term L^{B}_{lim}), which increased by up to +80% on day 8, and because of a more gradual increase in bacterial biomass (by up to +200% on day 20). Increasing DMS consumption by bacteria is the major contributor to the significant decrease in DMS seen after day 5. To some extent, the model behaviour in the Southern Ocean in response to iron addition is very similar to the observations made in the subarctic Pacific during the SERIES experiment, both for the DMS evolution and for the mechanisms that explain this evolution (Levasseur et al., 2006).

It is also noteworthy that although PISCES predicts little variability in terms of the chlorophyll and pCO_2 response to iron addition, there is a large predicted variability in the DMS response, from 0 to +3 nM among the different fertilized sites (Fig. 4). This illustrates the complex response of the DMS cycle to iron addition and the complex interplay between DMS source and sink processes.

3.3. Long-term iron fertilization of the Southern Ocean

To assess the long-term impact of a large-scale, artificial iron fertilization of the Southern Ocean on DMS emissions, we performed a 20-yr simulation with PISCES.

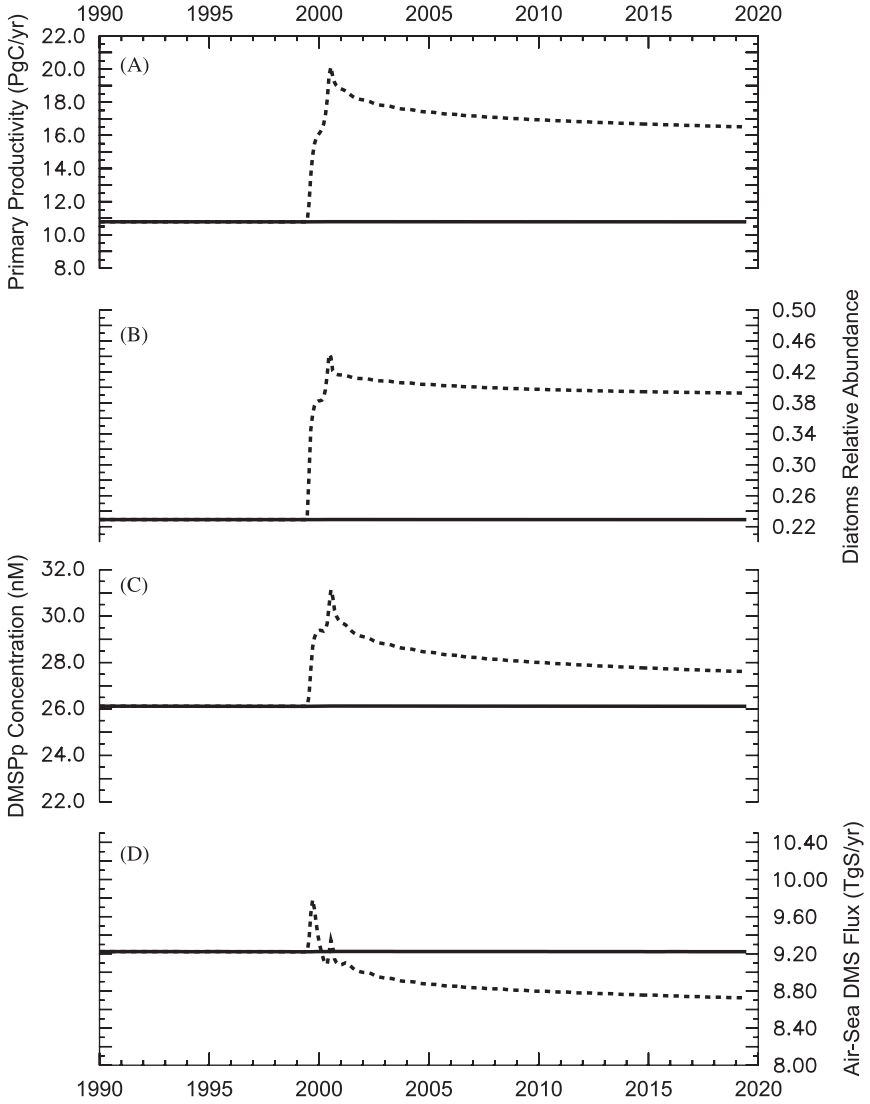

Fig. 5. Effects of iron fertilization on biogeochemical parameters and variables of the PISCES model. (A) Simulated annual mean primary production, (B) relative abundance of diatoms, (C) pDMSP concentration, (D) air–sea DMS flux for the control simulation (solid lines) and the fertilized experiment (dashed lines).

Iron is supplied continuously throughout the Southern Ocean (south of 40°S) mixed layer, such that it no longer limits productivity. Again, a similar experimental design was put forward by Aumont and Bopp (2006) and we recall some of the main results herein. During the first year, integrated primary production (PP, over the latitudinal band 30–80°S) increases from 11 to $>20\,\mathrm{pg\,C\,yr^{-1}}$. PP then decreases slowly to $16\,\mathrm{pg\,C\,yr^{-1}}$ by the end of the simulation (Fig. 5A). Both nanophytoplankton and diatom biomasses increase, but the relative increase in diatoms is greater (from 25% to >40% of total PP, Fig. 5B). This increase in the relative contribution of diatoms causes an only modest buildup in pDMSP concentration (from 26 to <28 nM, Fig. 5C). The 30–80°S DMS flux to the atmosphere increases during the first year of the experiment (from 9.2 to $>10\,\mathrm{Tg\,S\,yr^{-1}}$), but then decreases gradually to $8.7\,\mathrm{Tg\,S\,yr^{-1}}$, lower than in the control simulation (Fig. 5D). This is due to the modest buildup in pDMSP (only +5%, whereas PP increases by almost 50% after 20 yr of Fe fertilization), and to the increase in DMS-consumption rates (+31%) that results from higher levels of bacterial production (this increase in bacterial consumption is mainly driven by a 34% increase in bacterial biomass).

This small reduction in DMS flux conceals large latitudinal heterogeneities. PISCES predicts that a decrease in DMS concentrations north of 60°S is partly counterbalanced by a moderate increase around the Antarctic continent. The zonal means of chlorophyll, relative abundance of diatom, DMSP and DMS for the surface waters of the control and fertilized experiment illustrate three distinct latitudinal bands between 30°S and 80°S (Fig. 6). (1) North of 45°S, PISCES simulates almost no change in chlorophyll and in the relative abundance of diatoms, but a significant decrease in pDMSP and DMS. The S/C ratio of the nanophytoplankton decreases in response to iron addition. pDMSP (and subsequently DMS) concentrations are reduced. (2) Between 45°S and 60°S, the modelled ecosystem strongly responds to the iron fertilization by a large increase in chlorophyll (>+100%) and in the relative abundance of diatoms (from 30% to almost than 50%). These changes only translate into a modest pDMSP increase (+20%) and almost no changes in DMS concentrations. The large shift from nanophytoplankton to diatoms results in a significant decrease of the mean S/C ratio of the phytoplanktonic ecosystem. A large increase in the bacterial consumption of DMS also plays an important role. (3) South of 60°S, the iron fertilization increases surface chlorophyll, with little changes in the diatoms relative abundance (that are already abundant in the control simulation). The decrease in the S/C ratio of the phytoplanktonic ecosystem is thus limited. These changes translate into a modest increase in DMS concentrations.

The decoupling between PP and DMS predicted by this study on long time scales is consistent with conclusion drawn from paleoclimate records. New evidence from ice cores also suggests a reduced role of iron in modulating DMS emissions in the Southern Ocean (Wolff et al., 2006).

Methanesulphonate (MSA) and non-sea-salt sulphate (nss SO_4^{2-}) in Antarctica are both considered to be predominantly derived from marine biogenic emission of DMS (Cosme et al., 2005). High glacial values of MSA have been used to suggest increased oceanic DMS emissions during the last glacial period (Legrand et al., 1991). The working hypothesis was that increased fluxes of iron to the Southern Ocean during glacial periods (Petit et al., 1999) resulted in increased marine productivity and DMS emissions. Wolff et al. (2006), on the contrary, suggest that the higher concentrations of MSA in snow from glacial periods reflect a different deposition mechanism and do not indicate the past production of DMS. In contrast to MSA, the nss SO_4^{2-} flux is stable, within about 20%, through the entire 740-kyr EPICA core record (Wolff et al., 2006). This suggests little change in DMS emissions

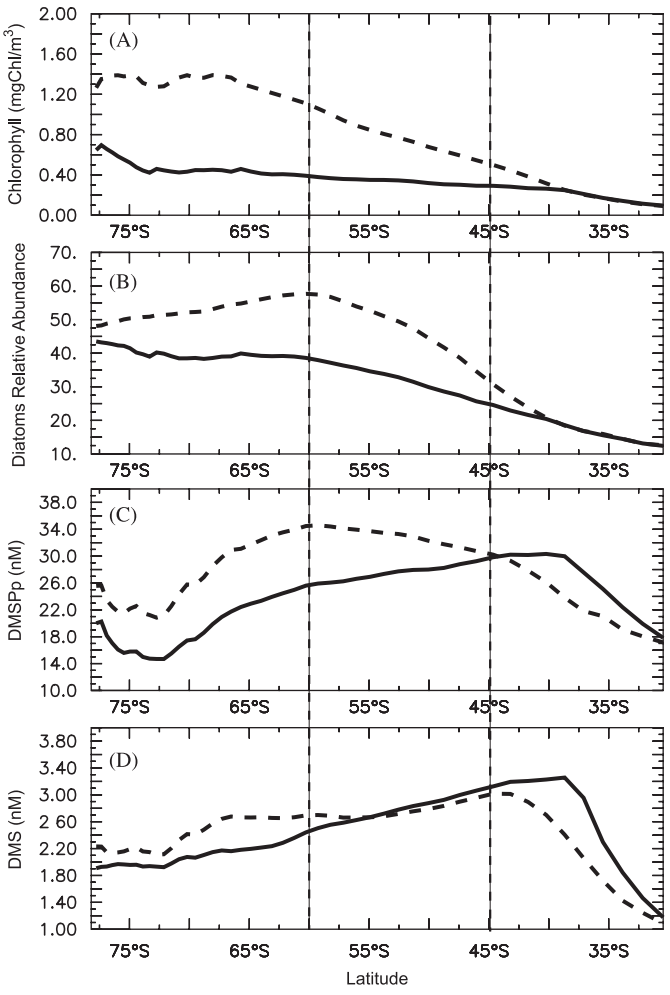

Fig. 6. Effects of iron fertilization on biogeochemical parameters and variables of the PISCES model. Zonal means of (A) Chl *a*, (B) diatoms relative abundance, (C) pDMSP and (D) DMS concentrations in surface waters of the Southern Ocean. Solid lines correspond to the climatological simulation and dashed lines correspond to the fertilized simulation after 20 yr of global-scale iron fertilization. Vertical lines are at 60°S and 45°S and separate regions of different DMS responses to iron addition.

over the last six glacial–interglacial cycles. Thus, even in the context of a significant increase in iron deposited to the Southern Ocean, no significant increase in DMS emissions over the Southern Ocean is recorded in the EPICA core.

4. Conclusion

Experimental results from both SOIREE (Turner et al., 2004 and KEOPS (Belviso et al., 2008) as well as the simulations over longer time scales presented here support the occurrence of a transient increase in the DMS source following Fe fertilization. Once the ecosystem has matured, the sources of DMS decline (due to a decrease in the S/C ratio of the phytoplanktonic ecosystem and a decrease in the transfer efficiency of DMSP to DMS) and the sinks of DMS increase (due a higher bacterial consumption rate). These processes act together to prevent the accumulation of DMS in water. Our modelling exercise should not be taken as a prediction, but it suggests that iron fertilization of the Southern Ocean would not act to increase DMS fluxes from the ocean and hence would not amplify cooling that might result if there were an associated increased in oceanic uptake of carbon dioxide. Lastly, we suggest that increased Fe deposition over glacial–interglacial cycles would probably not increase DMS emissions from the Southern Ocean.

Acknowledgments

We thank Alessandro Tagliabue for his help to improve the manuscript. We thank two anonymous reviewers for their comments and suggestions. The KEOPS project was supported by INSU and IPEV. The ISLAND project was supported by INSU. CPU hours have been provided by CEA/CCRT (Project p48) and CNRS/IDRIS (Project i060040). This is LSCE contribution no. 2433.

References

Anderson, T.R., Spall, S.A., Yool, A., Cipollini, P., Challenor, P.G., Fasham, M.J.R., 2001. Global fields of sea surface dimethylsulfide predicted from chlorophyll, nutrients and light. Journal of Marine Systems 30, 1–20.

Aumont, O., Bopp, L., 2006. Globalizing results from ocean in-situ fertilization experiments. Global Biogeochemical Cycles 20 (2).

Aumont, O., Belviso, S., Monfray, P., 2002. Dimethylsulfoniopropionate (DMSP) and dimethylsulfide (DMS) sea surface distributions simulated from a global three-dimensional ocean carbon cycle model. Journal of Geophysical Research 107 (C4), 3029.

Bakker, D.C.E., Watson, A.J., Law, C.S., 2001. Southern Ocean iron enrichment promotes inorganic carbon drawdown. Deep-Sea Research II 48 (11–12), 2483–2507.

Bell, T.G., Malin, G., McKee, C.M., Liss, P.S., 2006. A comparison of dimethylsulphide (DMS) data from the Atlantic Meridional Transect (AMT) programme with proposed algorithms for global surface DMS concentrations. Deep-Sea Research II 53, 1720–1735.

Belviso, S., Morrow, R., Mihalopoulos, N., 2000. An atlantic meridional transect of surface water dimethyl sulfide concentrations with 10–15 km horizontal resolution and close examination of ocean circulation. Journal of Geophysical Research 105, 14423–14431.

Belviso, S., Bopp, L., Moulin, C., Orr, J.C., Anderson, T.R., Chu, S., Elliott, S., Maltrud, M.E., Simo, R., 2004. Comparison of global climatological maps of sea surface dimethylsulfide. Global Biogeochemical Cycles 18 (3).

Belviso, S., Bopp, L., Mosseri, J., Tedetti, M., Garcia, N., Griffiths, B., Joux, F., Obernosterer, I., Uitz, J., Veldhuis, M.J.W., 2008. Effect of natural iron fertilization on the distribution of DMS and DMSP in the Indian sector of the Southern Ocean. Deep-Sea Research II, this issue [doi:10.1016/j.dsr2.2007.12.040].

Bopp, L., Kohfeld, K.E., Le Quéré, C., Aumont, O., 2003. Dust impact on marine biota and atmospheric pCO_2 during glacial periods. Paleoceanography 18 (2).

Bopp, L., Boucher, O., Aumont, O., Belviso, S., Dufresne, J.-L., Pham, M., Monfray, P., 2004. Will marine dimethylsulfide concentrations amplify or alleviate global warming? A model study. Canadian Journal of Fisheries and Aquatic Sciences 61, 673–684.

Bopp, L., Aumont, O., Cadule, P., Alvain, S., Gehlen, M., 2005. Response of diatoms distribution to global warming and potential implications: a global model study. Geophysical Research Letters 32 (19).

Boyd, P.W., Watson, A.J., Law, C.S., et al., 2000. A mesoscale phytoplankton bloom in the polar Southern Ocean stimulated by iron fertilization. Nature 407 (6805), 695–702.

Bucciarelli, E., Sunda, W.G., 2003. Influence of CO_2, nitrate, phosphate and silicate limitation on intracellular DMSP in batch cultures of the coastal diatom Thalassiosira pseudonana. Limnology and Oceanography 48, 2256–2265.

Bucciarelli, E., Sunda, W.G., Belviso, S., Sarthou, G., 2007. Impact of the diel cycle on the production of dimethylsulfoniopropionate in batch cultures of *Emiliania huxleyi*. Aquatic Microbial Ecology 48, 73–81.

Charlson, R.J., Lovelock, J.E., Andreae, M.O., Warren, S.G., 1987. Oceanic phytoplankton, atmospheric sulphur, cloud albedo and climate. Nature 326, 655–661.

Chu, S., Elliott, S., Maltrud, M.E., 2003. Global eddy permitting simulations of surface ocean nitrogen, iron, sulfur cycling. Chemosphere 50, 223–235.

Cosme, E., Hourdin, F., Genthon, C., Martinerie, P., 2005. Origin of dimethylsulfide, non-sea-salt sulfate, and methanesulfonic acid in eastern Antarctica. Journal of Geophysical Research 110, D03302.

de Baar, H.J.W., Boyd, P.W., Coale, K.H., et al., 2005. Synthesis of iron fertilization experiments: From the Iron Age in the Age of Enlightenment. J. Geophys. Res. 110, C09S16.

Eppley, R.W., 1972. Temperature and phytoplankton growth in the sea. Fishery Bulletin 70, 1063–1085.

Erickson III, D.J., Ghan, S.J., Penner, J.E., 1990. Global ocean-to-atmosphere dimethylsulfide flux. Journal of Geophysical Research 95, 7543–7552.

Fichefet, T., Morales Maqueda, M.A., 1997. Sensitivity of a global sea ice model to the treatment of ice thermodynamics and dynamics. Journal of Geophysical Research 102, 12,609–12,646.

Gall, M.P., Boyd, P.W., Hall, J., et al., 2001. Phytoplankton processes. Part 1: community structure during the Southern Ocean Iron RElease Experiment (SOIREE). Deep-Sea Research II 48 (11–12), 2551–2570.

Gorgues, T., Menkes, C., Aumont, O., Vialard, J., Dandonneau, Y., Bopp, L., 2005. Biogeochemical impact of tropical instability waves in the equatorial Pacific. Geophysical Research Letters 32 (24), 10.

Gunson, J.R., Spall, S.A., Anderson, T.R., et al., 2006. Climate sensitivity to ocean dimethylsulphide emissions. Geophysical Research Letters 33 (7).

Kettle, A.J., Andreae, M.O., 2000. Flux of dimethylsulfide from the oceans: a comparison of updated data sets and flux models. Journal of Geophysical Research 105, 26793–26808.

Kettle, A.J., et al., 1999. A global database of sea surface dimethylsulfide (DMS) measurements and a procedure to predict sea surface DMS as a function of latitude, longitude, and month. Global Biogeochemical Cycles 13, 399–444.

Kieber, D.J., Jiao, J., Kiene, R.P., Bates, T.S., 1996. Impact of dimethyl sulfide photochemistry on methyl sulfur cycling in the equatorial Pacific Ocean. Journal of Geophysical Research C 101, 3715–3722.

Kiene, R.P., Linn, L.J., Bruton, J.A., 2000. New and important roles for DMSP in marine microbial communities. Journal of Sea Research 43, 209–224.

Larsen, S.H., 2005. Solar variability, dimethyl sulphide, clouds, and climate. Global Biogeochemical Cycles 19.

Le Clainche, Y., et al., 2006. Modeling analysis of the effect of iron enrichment on dimethyl sulfide dynamics in the NE Pacific (SERIES experiment). Journal of Geophysical Research 111, C01011.

Lefèvre, M., Vézina, A., Levasseur, M., Dacey, J.W.H., 2002. A model of dimethylsulphide dynamics for the subtropical North Atlantic. Deep-Sea Research I 49, 2221–2239.

Legrand, M., et al., 1991. Ice-core record of oceanic emissions of dimethylsulphide during the last climate cycle. Nature 350, 144–146.

Legrand, M.R., Delmas, R.J., Charlson, R.J., 1998. Climate forcing implications from Vostok ice-core sulphate data. Nature 334, 418–420.

Levasseur, M., Scarratt, M.G., Michaud, S., Merzouk, A., Wong, C.S., Arychuk, M., Richardson, W., Wong, E., Marchetti, A., Kiyosawa, H., 2006. DMSP and DMS dynamics during a mesoscale iron fertilization experiment in the Northeast Pacific. Part I. Temporal and vertical distributions. Deep-Sea Research II 53 (20–22), 2353–2369.

Liss, P.S., Chuck, A., Bakker, D., Turner, S., 2005. Ocean fertilization with iron: effects on climate and air quality. Tellus 57, 269–271.

Madec, G., Delecluse, P., Imbard, M., Levy, C., 1998. OPA8.1 Ocean General Circulation Model Reference Manual, Notes du pôle de modélisation de l'IPSL.

Petit, J.R., Jouzel, J., Raynaud, D., Barkov, N.I., Barnola, J.M., Basile, I., Bender, M., Chappellaz, J., Davis, J., Delaygue, G., Delmotte, M., Kotlyakov, V.M., Legrand, M., Lipenkov, V., Lorius, C., Pépin, L., Ritz, C., Saltzman, E., Stievenard, M., 1999. Climate and Atmospheric History of the Past 420,000 years from the Vostok Ice Core, Antarctica. Nature 399, 429–436.

Saltzman, E.S., King, D.B., Holmen, K., Leck, C., 1993. Experimental determination of the diffusion coefficient of dimethylsulfide in water. Journal of Geophysical Research 98, 16481–16486.

Sciare, J., Mihalopoulos, N., Dentener, F., 2000. Interannual variability of atmospheric dimethylsulfide in the Southern Indian Ocean. Journal of Geophysical Research 105, 26369–26377.

Simó, R., Dachs, J., 2002. Global ocean emission of dimethylsulfide predicted from biogeophysical data. Global Biogeochemical Cycles 16 (4), 1078.

Simó, R., Pedros-Alio, C., 1999. Role of vertical mixing in controlling the oceanic production of dimethyl sulfide. Nature 402, 396–397.

Steffels, J., Steinke, M., Turner, S., Malin, G., Belviso, S., 2007. Environmental constraints on the production of the climatically active gas dimethylsulphide (DMS) and implications for ecosystem modeling. Biogeochemistry 83, 245–275.

Sunda, W., Kieber, D.J., Kiene, R.P., Huntsman, S., 2002. An antioxidant function for DMSP and DMS in marine algae. Nature 418, 317–320.

Taylor, K.E., 2001. Summarizing multiple aspects of model performance in a single diagram. Journal of Geophysical Research 106, 7183–7192.

Turner, S.M., Harvey, M.J., Law, C.S., Nightingale, P.D., Liss, P.S., 2004. Iron-induced changes in oceanic sulfur biogeochemistry. Geophysical Research Letters 31.

Vezina, A.F., 2004. Ecosystem modelling of the cycling of marine dimethylsulfide: a review of current approaches and of the potential for extrapolation to global scales. Canadian Journal of Fisheries and Aquatic Sciences 61, 845–856.

Wanninkhof, R., 1992. Relationship between wind speed and gas exchange over the ocean. Journal of Geophysical Research 97, 7373–7382.

Wingenter, O.W., Haase, K.B., Strutton, P., Friederich, G., Meinardi, S., Blake, D.R., Rowland, F.S., 2004. Changing concentrations of CO, CH_4, C_5H_8, CH_3Br, CH_3I, and dimethyl sulfide during the Southern Ocean iron enrichment experiments. Proceedings of the National Academy of Sciences of the United States of America 101, 8537–8541.

Wolff, E.W., et al., 2006. Southern Ocean sea-ice extent, productivity and iron flux over the past eight glacial cycles. Nature 440, 491.